Analyst

PAPER

Cite this: *Analyst*, 2014, **139**, 6529

Sensitive impedimetric biosensor based on duplex-like DNA scaffolds and ordered mesoporous carbon nitride for silver(I) ion detection†

Yaoyu Zhou,[ab] Lin Tang,*[ab] Xia Xie,[ab] Guangming Zeng,*[ab] Jiajia Wang,[ab] Yaocheng Deng,[ab] Guide Yang,[ab] Chen Zhang,[ab] Yi Zhang[ab] and Jun Chen[ab]

Received 31st August 2014
Accepted 11th October 2014

DOI: 10.1039/c4an01607f

www.rsc.org/analyst

This study demonstrates a new, unlabeled immobilized DNA-based biosensor with ordered mesoporous carbon nitride material (MCN) for the detection of Ag^+ by electrochemical impedance spectroscopy (EIS) with $[Fe(CN)_6]^{4-/3-}$ as the redox couple. The unlabeled immobilized DNA initially formed the hairpin-like structure through hybridization with the probe, and then changed to duplex-like structure upon interaction with Ag^+ in solution to form a C–Ag^+–C complex at electrode surface. As a result, the interfacial charge-transfer resistance of the electrode towards the $[Fe(CN)_6]^{4-/3-}$ redox couple was changed. Thus, a declined charge transfer resistance (R_{ct}) was obtained, corresponding to Ag^+ concentration. MCN provide an excellent platform for DNA immobilization and faster electron transfer. Impedance data were analyzed with the help of Randles equivalent circuit. The lower detection limit of the biosensor for Ag^+ is 5×10^{-11} M with good specificity. All results showed that this novel approach provides a reliable method for Ag^+ detection with sensitivity and specificity, potentially useful for practical applications. Moreover, other DNA detection methods for more heavy metals may be obtained from this idea and applied in the environmental field.

Introduction

Silver(I) ions are recognized to be one of the most hazardous metal pollutants because of their potential toxicity to human health and the environment, surpassed only by mercury.[1] They are mostly generated by the photographic and imaging industry, dental and medical products, electrical and electronic equipment, and other products such as jewelry, coins, and mirrors.[2] Their toxicity may accumulate in the human body through the food chain or drinking, bringing on undesirable, seriously damaging problems, such as cytotoxicity, organ failure and reduction in mitochondrial function.[3] Thus, it is of great significance to monitor the level of silver(I) ion in natural water environment worldwide. Traditional quantitative methods, such as electrothermal atomic absorption spectrometry (ETAAS),[4] inductively coupled plasma mass spectrometry,[5] and cold vapor atomic fluorescence spectrometry (CVAFS),[6] have been extensively applied to detect heavy metal ions with high sensitivity. In addition to the time-consuming processes and expensive, complex instrumentation required, these techniques normally involve sophisticated chemical procedures for extracting metal ions from samples, in which the speciation change of metal ions is unavoidable.[7]

In the past decade, several efforts have been made to the design a DNA-based biosensors to detect metal ions based on interactions between some metal ions and nucleic acids to form stable metal-mediated DNA duplexes.[8] For example, mercury ions (Hg^{2+}) are capable of selectively coordinating thymine (T) bases to form stable T–Hg^{2+}–T complexes.[9] For Pb^{2+} detection, most sensors are based on the Pb^{2+}-dependent DNAzyme and the Pb^{2+}-stabilized G-quadruplex.[10] In addition, since Ono *et al.* determined that Ag^+ can selectively coordinate cytosine (C) bases to form a stable C–Ag^+–C complex and discussed the mechanism of the specific interactions between silver(I) ions and cytosine–cytosine pairs,[11] various detection techniques, such as fluorescence, surface-enhanced Raman spectroscopy, resonance scattering, colorimetry and electrochemical methods, have been applied to selectively detect Ag^+ in aqueous media by taking advantage of specific C–Ag^+–C interaction and signal amplification of nanomaterials.[11–13] Accordingly, various detection techniques were applied to selectively detect these heavy metal ions based on a hairpin-like structure DNA biosensor.[11,14,15] Compared to linear DNA structures, hairpin-like structure DNA biosensors have higher detection sensitivity and stability,[16] generally specific to a given ligand–biomolecule

[a]*College of Environmental Science and Engineering, Hunan University, Ministry of Education, Changsha 410082, China. E-mail: tanglin@hnu.edu.cn; Fax: +86-731-88822778; Tel: +86-731-88822778*

[b]*Key Laboratory of Environmental Biology and Pollution Control (Hunan University), Ministry of Education, Changsha 410082, PR China. E-mail: zgming@hnu.edu.cn*

† Electronic supplementary information (ESI) available: More details about the optimization of DNA-based biosensor, the reproducibility of the biosensor, electrodeposition of L-Lys, analysis the Ag^+ in real samples, SEM and TEM images of MCN. See DOI: 10.1039/c4an01607f

interface and mostly insensitive to other molecules, even in complex environments (natural water, living cells, or blood serum) because of their highly constrained conformations,[17] which may improve the potential application in a real environment. Moreover, an effective immobilization platform for the DNA scaffold is also a key issue in the detection system. To date, various nanomaterials, such as GNPs/carbon nanodots,[18] single-walled carbon nanotubes (SWCNTs),[19] carbon nanotube (CNT),[20] porous materials (micropores (<2 nm), mesopores (2 ± 50 nm) and macropores (>50 nm)),[21,22] have been successfully used as an effective platform for sensors relying on different transduction schemes. In our previous study, we used ordered mesoporous carbon nitride (MCN) as the platform for electrochemical biosensors, which can obviously increase the sensitivity and lower the detection limit.[23] MCN has a better microenvironment for immobilized biomolecules due to the CN matrix, higher affinity for the bioactivator, and faster electron transfer between bioactivator and MCN-sensing sites because of the π–π* electronic transition in the MCN.

This study developed a novel impedimetric hairpin-like structure DNA biosensor with MCN for the ultrasensitive detection of Ag^+. The interfacial charge-transfer resistance of the DNA/MCH/GNPs–MCN/L-Lys-modified electrode will change upon the hybridization of surface–tethered probe DNA with its complementary DNA and interaction with Ag^+ in solution, which could be useful for the practical determination of Ag^+.

Experimental

Chemicals and reagents

Pluronic copolymer P123 (EO20PO70EO20, EO = ethylene oxide, PO = propylene oxide) and tris(hydroxymethyl)aminomethane, were purchased from Sigma-Aldrich (USA). Gold(III) chloride trihydrate ($HAuCl_4 \cdot 3H_2O$, 99.9%) was purchased from Dingguo Biotechnology Co., Ltd (Shanghai, China). Tetraethoxysilane (TEOS), $K_3[Fe(CN)_6]$, $K_4[Fe(CN)_6]$, L-lysine (L-Lys), $AgNO_3$, $NaClO_4$, and all other chemicals were of analytical grade and used as received. All the aqueous solutions were prepared using ultrapure water (18 MΩ cm, Milli-Q, Millipore). Tris–ClO_4 buffer (pH = 7.4) containing 300 mM $NaClO_4$ and phosphate buffer saline (PBS, 0.1 M KH_2PO_4 and 0.1 M Na_2HPO_4) were used in this work. The DNA target-specific probes used for hybridization in our experiment were synthesized by Sangon (Shanghai, China) and purified using high performance liquid chromatography. The sequences of the oligonucleotides include.

5′–HS–$(CH_2)_6$–SS–$(CH_2)_6$–TCA–GAC–TAGC–CCC–CCC–CCC–CCC–GG–ACG–3′ (S1)

5′–CC–TGC–TTT–CGT–CC–3′ (S2)

3′–AGT–CTG–ATCG–CCC–CCC–CCC–CCC–GG–ACG–5′ (S3)

Apparatus

Cyclic voltammetric (CV) measurement and electrochemical impedance spectroscopy (EIS) measurements were carried out on CHI760D electrochemical workstation (Chenhua Instrument, Shanghai, China). The three-electrode system used in this study consisted of a modified electrode as working electrode, a saturated calomel electrode (SCE) as reference electrode and a Pt foil auxiliary electrode. The pH of the solution was measured with a model PHSJ-3 digital acidimeter (Shanghai Leici Factory, China). Scanning electron microscopy (SEM) images were obtained using a JSM-6360LV field emission scanning electron microscope. Transmission electron microscopy (TEM) images were obtained on a JEOL 1230 electron microscope operated at 100 kV. A Sigma 4 K 15 laboratory centrifuge, a vacuum freezing dryer and a mechanical vibrator were used in the assay.

Sensor fabrication

The MCN was synthesized in our laboratory as previously described.[23] The bare glass carbon electrode (GCE) used for the self-assembled monolayer was first polished in an alumina slurry, rinsed with deionized water, and then etched for about 10 min in a "Piranha" solution (98% H_2SO_4 : 30% H_2O_2 = 3 : 1 (v/v)) to remove organic contaminants (**Caution**: Piranha solution reacts violently with organic materials, thus should be handled with extreme care).[23–25] Finally, the electrode surface was treated by cyclic voltammetry scan in 0.5 M H_2SO_4 between 0 and 1.2 V at the scan rate of 50 mV s^{-1} until a reproducible scan was obtained.

The MCN suspension was prepared by dispersing 1 mg purified MCN into 1 mL *N*,*N*-dimethylformamide with the aid of ultrasonic agitation. The preparation of GNPs–MCN/L-lysine/GCE was carried out as follows (Scheme 1): initially, the L-Lys film modified electrode was obtained in L-Lys electrodeposition process (Fig. S-1†). Then, a 5.0 μL of the MCN dispersion was dip coated onto L-lysine/GCE. The electrode (MCN/L-lysine/GCE) was dried at room temperature (25 °C) for about an hour. The GNPs were immobilized on the pretreated electrode (MCN/L-lysine/GCE) by electrodepositing gold(III) chloride trihydrate ($HAuCl_4 \cdot 3H_2O$); the method of electrodeposition was used according to the previous description in our laboratory.[24] Subsequently, the mixture solution of 10 μL S1 probe was dropped onto the electrode surface and maintained at 4 °C for self-assembly through thiol–gold bonding for 10 h. The hybridization of the biosensor is as follows: the modified electrode with S1 probes coated was immersed into 400 μL of 6-

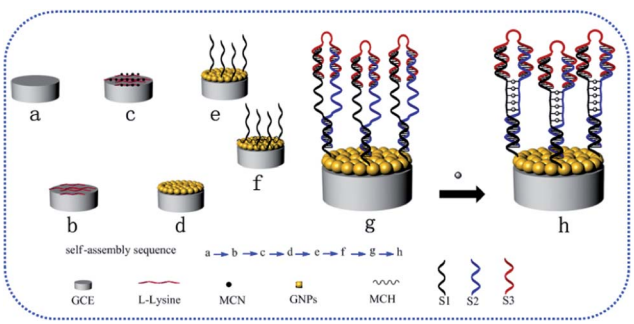

Scheme 1 The fabrication processes of the duplex-like DNA scaffolds biosensor.

mercapto-1-hexanol (MCH) solution for 1 h to improve the quality and stability, to reduce nonspecific adsorption of DNA and to obtain a well-aligned DNA monolayer. Then, the electrode was soaked in the 2.5 μM DNA solution containing S2 and S3 (1 : 1), and incubated at room temperature for 1 h to form the hairpin-like structured (S1 + S2 + S3). Subsequently, it was washed with Tris–ClO_4 buffer (pH = 7.4). When not in use, the electrode was stored in a moist state at 4 °C.

Design of the biosensing strategy

Scheme 1 outlines the preparation processes of the duplex-like DNA scaffolds biosensor. Here, MCN was synthesized and applied to fix DNA through Au nanoparticle (GNPs) films as a transducer to convert the recognition information into a detectable signal. GNPs were also employed to amplify the detectable signal, which can also easily and directly couple mercapto biomolecules with no further modification. L-lysine (L-Lys) was also used for its non-toxicity, biocompatibility, and good film-forming ability. First, MCN enriched in amino and carboxy groups could be immobilized on the electrode surface by linking the $-NH_2$ and –COOH of L-Lys through amino–carboxyl bonding,[23] and used as carrier for loading DNA labels and accelerating electron-transfer. The spatial structure of the MCN/GNPs offered more reaction sites and space for self-assembly of the DNA probe because of the CN matrix; the CN matrix has many prominent properties, especially the presence of basic sites, affinity for biomolecules and larger bioactivity after an entrapment procedure,[23] which are important for biosensor performance. Second, the use of low concentration L-Lys protected the link between MCN/GNPs and GCE by forming a film. They can more tightly fix the MCN/GNPs film through its amino–carboxyl as molecular bridge; this method might extend the usable life and stability of the biosensor. Third, the film structure of MCH on the electrode surface was similar to the reported function of chitosan[26] and polyethylene glycol (PEG),[27] weakening non-specific adsorptions, strengthening the orientation of the thiolated DNA probe, and facilitating the hybridization process.[28] Though L-Lys and MCH reduced electric conductivity and blocked the electron transfer processes at the electrode surface, their advantages outweighed the disadvantages here.

Detection process

The electrode reacted with various concentrations of Ag^+ in buffers (Tris–ClO_4 buffer, pH 7.4) for 2 h. Subsequently, it was washed with Tris–ClO_4 buffer (pH = 7.4). A conventional three-electrode system was used, and all the measurements were carried out at room temperature. Electrochemical impedance spectroscopy (EIS) was performed in 0.1 M PBS (pH 7.4) containing 5 mM $[Fe(CN)_6]^{3-/4-}$ (1 : 1) and 10 mM KCl in the frequency range from 0.1 Hz to 100 kHz with 5 mV as the amplitude at a polarization potential of 0.18 V. All the measurements were repeated minimum three times with separate electrodes to obtain statistically meaningful results.

Results and discussion

Mechanism of duplex-like DNA structure for Ag^+ ions detection

Scheme S-1† illustrates the mechanism of this biosensor. The single strand oligonucleotide S1 anchored the composite GNPs/MCN/L-Lys/GCE platform by the Au–S covalent bond, which is ready for the hybridization with S2 and S3, to form a stable hairpin-like structure. $[Fe(CN)_6]^{3-/4-}$, a redox pair, is frequently used as a redox indicator for the electrode kinetics at the interface (as shown in Scheme S-1†). Upon the hybridization of surface-tethered probe DNA with its complementary probes in solution, the interfacial charge-transfer resistance for the negatively charged $[Fe(CN)_6]^{3-/4-}$ redox probe on the electrode is remarkably increased due to the formation of hairpin-like structure.

Then, the interfacial charge-transfer resistance as the hairpin-like structure is changed to duplex-like structured upon DNA interaction with Ag^+ in solution to form a C–Ag^+–C complex at the electrode surface. Fig. 1 shows the representative Nyquist plots of the EIS spectra before and after hybridization with probes (S1 + S2 + S3), and after incubation in the solution

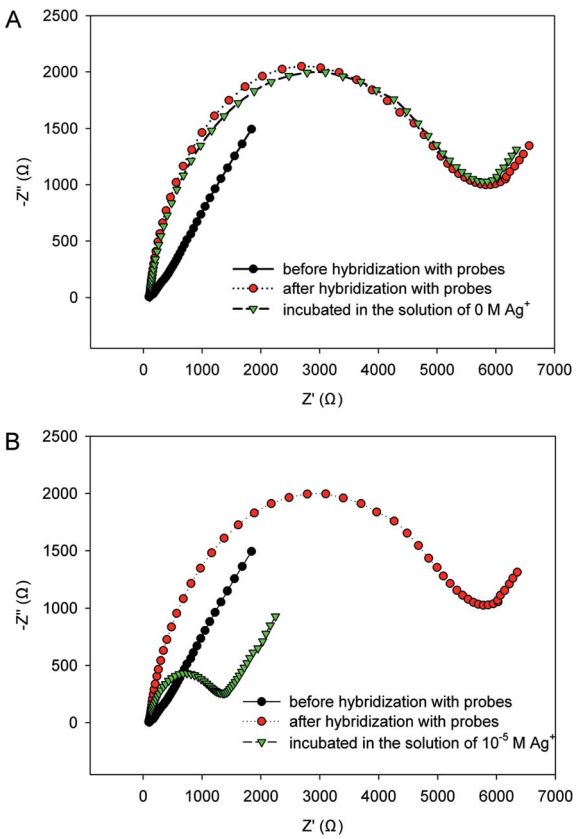

Fig. 1 Nyquist plots for the faradaic impedance measurement before and after hybridization with probes (S1 + S2 + S3), and after incubation in the solution of (A) 0 M and (B) 10^{-5} M Ag^+ in PBS (0.1 M, pH 7.4) containing 5 mM $[Fe(CN)_6]^{3-/4-}$ (1 : 1) and 10 mM KCl, in the frequency range from 0.1 Hz to 100 kHz with 5 mV as the amplitude at a polarization potential of 0.18 V.

of 0 M Ag^+ (Fig. 1A) and 10^{-5} M Ag^+ (Fig. 1B). It can be clearly observed that the impedance increased after hybridization with probes (S1 + S2 + S3) and shifted back in the presence of Ag^+ (10^{-5} M). In fact, the difference of the charge transfer resistance (ΔR_{ct}) of DNA films in the presence and absence of the metal ion was dependent on the concentration of the given metal ion.[29] The result also coincides with the presumed mechanism about the silver-induced conformational change of hairpin-like structure to duplex-like structure, thus enhancing the electron transfer. The different charge and conformational characteristics of DNA on the surface led to different charge-transfer resistances for the redox indicator ions.[29,30] On the basis of the results discussed above, the interactions between DNA and Ag^+ led to the decrease of R_{ct}, which could be used for the detection of Ag^+.

Characterization of MNC and electrode assembly process

The SEM and TEM images of MCN are shown in Fig. S-2.† As can be seen in Fig. S-2A,† MCN formed a chained rod structure, which was evenly dispersed on the surface of GCE. Fig. S-2B† clearly presented a hexagonal arrangement of the mesopores. Furthermore, the Fourier-transform infrared (FTIR) spectrum, which was presented in our previous work,[23] showed that the MCN was enriched in amino. Thus, the amino group could make the MCN/L-lysine more stable.

To test the performance of the modified electrode, CV was carried out in phosphate buffer (pH 7.4) containing 5 mM $[Fe(CN)_6]^{3-/4-}$ (1 : 1) and 10 mM KCl to test the properties of the modified electrode. As can be seen in Fig. 2, the immobilization of L-Lys on the GCE led to a significant decrease in peak current of the redox probe. After modification with MCN and GNPs, the peak current obviously increased and the peak potential difference reached the minimum. These cyclic voltammograms proved that the modified electrode had a good current response capability.

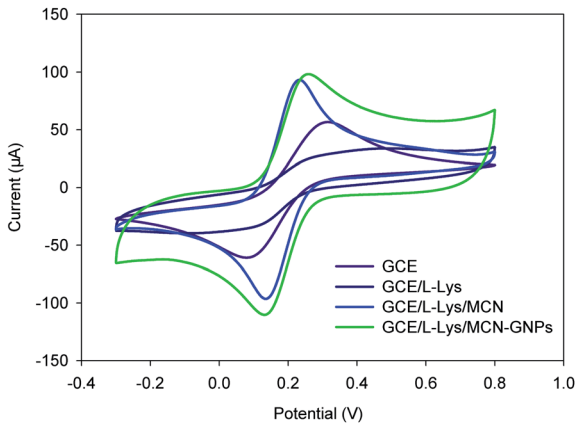

Fig. 2 Cyclic voltammetry diagrams of GCE, GCE/L-Lys, GCE/L-Lys/MCN, GCE/L-Lys/MCN–GNPs, using a 10.0 mM KCl solution containing 5.0 mM $[Fe(CN)_6]^{4-/3-}$, with potential range of −0.3 to 0.8 V, and a scan rate of 100 mV s^{-1}.

Optimization of the variables of experimental conditions

The experimental conditions were optimized before the quantitative analysis of Ag^+. Fig. S-3A† demonstrated the effect of self-assembly time of capture probe (S1) on the modified electrode surface. The ΔR_{ct} increased with the self-assembly time, and then reached a plateau at 10 h. Therefore, the self-assembly time of 10 h was used in the subsequent measurements. Similarly, the optimization of hybridization conditions includes the hybridization time of DNA hybridization (S2 + S3) reaction. The hybridization time is an important factor that ensures the adequacy of a contact reaction. The response current sharply increased with the hybridization time increasing from 30 to 60 min, and then leveling off (Fig. S-3B†). The time course of the Ag^+ complexing with C bases was studied by the electrochemical response signal to optimize the time to obtain the maximum loading of Ag^+ on the sensor interface (Fig. S-3C†). The experimental data indicates that incubation time has a significant effect on the response signal, which indicates that the adsorption quantity of Ag^+ considerably relies on the time accretion. The ΔR_{ct} enlarged as the incubation time increased and remained constant at a saturation value after about 120 min, indicating that an incubation time of 120 min is absolutely sufficient. Accordingly, the sensor was incubated in Ag^+ ion solution for 120 min in all subsequent analyses.

Analytical properties of the impedimetric DNA biosensor

The measured EIS data can be fitted with an equivalent circuit, as shown in Scheme S-1c.† This equivalent circuit consists of the electron-transfer resistance (R_{ct}), the Warburg impedance (Z_w), the ohmic resistance of the electrolyte (R_s), and interfacial capacitance (C_{dl}). EIS includes a semicircular part and a linear part. The semicircle diameter could represent the electron-transfer resistance (R_{ct}), the polarization resistance at an equilibrium potential, which is utilized as a main indicator in the EIS detection. The measured data and the fitting curve shown in Fig. 3 are the EIS fitting plots of the electrode (after hybridization with S1 + S2 + S3) using the above equivalent circuit shown in Scheme S-1c.† The various elements of the equivalent circuit were obtained, and the plot fitting and the fitting errors were less than 6.0%. The good agreement between the measured data and the fitting curve indicates that this equivalent circuit is suitable and meaningful for this electrochemical system. Therefore, this equivalent circuit is used to fit the impedance spectroscopy data and extract the values of the equivalent circuit elements. The impedance spectra for all the system were analyzed using the Randles equivalent circuit.

Fig. 4A displays the Nyquist plots obtained with the modified electrode in 0.1 M PBS (pH 7.4) containing 5 mM $[Fe(CN)_6]^{3-/4-}$ (1 : 1) and 10 mM KCl after the electrode was incubated with different concentrations of Ag^+ under the optimized experimental conditions (as shown in Fig. S-3†). As shown in Fig. 4A, upon decreasing the concentration of Ag^+ from 10^{-10} M to 10^{-5} M, only a part of C–C mismatches could react with Ag^+ to form C–Ag^+–C, which led to the decrease in ΔR_{ct} (Table S-1†). The change in the R_{ct} was linear with the logarithm of the concentration of Ag^+ within a concentration range from 10^{-10} M to

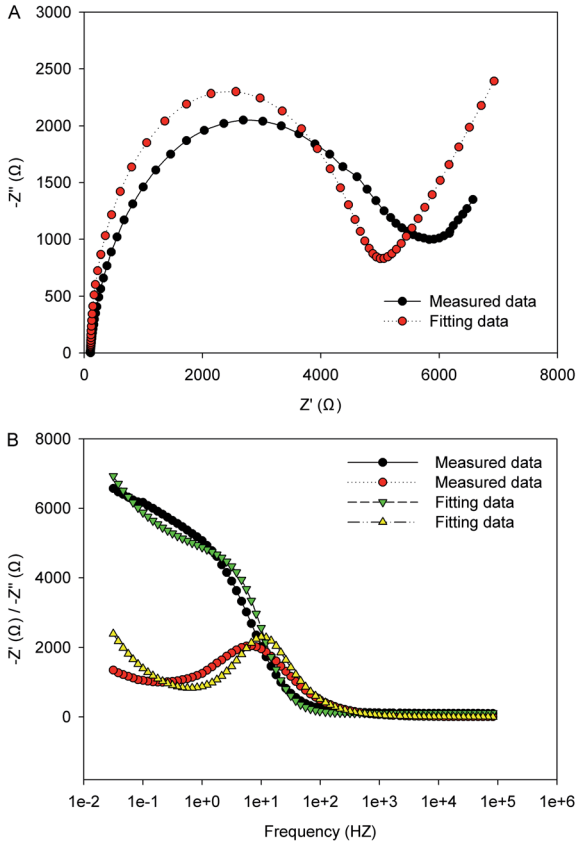

Fig. 3 (A) Nyquist plots of electrochemical impedance spectroscopy of the electrode (after hybridization with S1 + S2 + S3) together with the fitting data. (B) Real and image plots of electrochemical impedance spectroscopy of the electrode (after hybridization with S1 + S2 + S3).

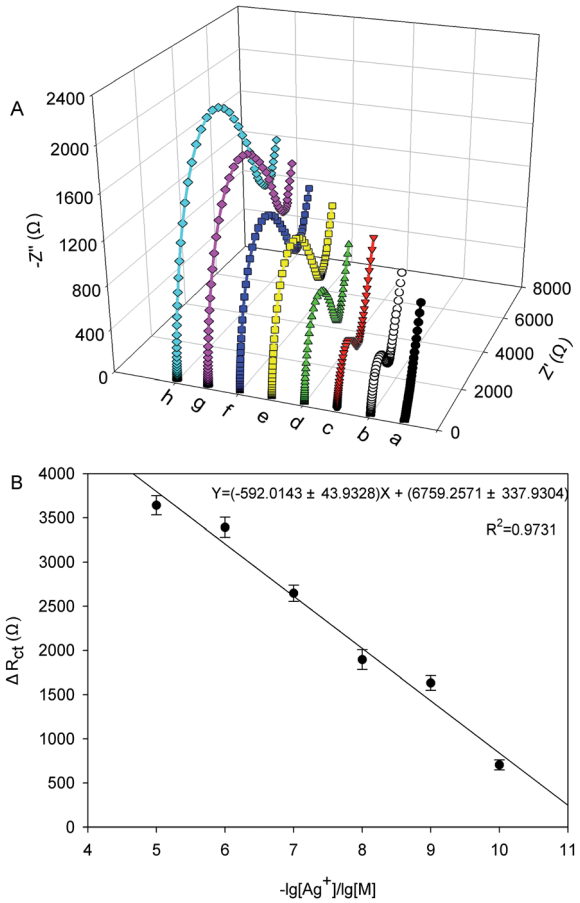

Fig. 4 (A) A series of Nyquist plots before hybridization (a), after hybridization with DNA (S1 + S2 + S3) and incubation in 1×10^{-5} M (b),1×10^{-6} M (c), 1×10^{-7} M (d), 1×10^{-8} M (e), 1×10^{-9} M (f) and 1×10^{-10} M (g) Ag^+, and after hybridization with DNA (S1 + S2 + S3) (h). (B) The plot of ΔR_{ct} *vs.* Ag^+ concentration ranging from 1×10^{-10} $M^{-1} \times 10^{-5}$ M. Error bars indicate standard deviations from three replicative tests.

10^{-5} M. The linear regression equation was $Y = (-592.0143 \pm 43.9328)X + (6759.2571 \pm 337.9304)$ (Y is the ΔR_{ct} (Ω); X is the common logarithmic value of the target concentration (M)) with a correlation coefficient $R^2 = 0.97$. The detection limit of the impedimetric DNA biosensor was estimated to be 5×10^{-11} M, based on $S/N = 3$. The proposed biosensor exhibited improved analytical performances in terms of linear detection range and showed a lower detection limit. The limit of detection was competitive with other highly sensitive detection approaches such as fluorescence, colorimetry and electrochemical methods, as presented in Table 1.

The stability, reproducibility and selectivity of the biosensor

The repeatability of the same biosensor was examined by detecting 1×10^{-8} M Ag^+ in 0.1 M PBS (pH 7.4) containing 5 mM $[Fe(CN)_6]^{3-/4-}$ (1 : 1) and 10 mM KCl using the EIS technique (Fig. 5). A relative standard deviation (R.S.D.) value of 4.1% was obtained for three determinations, which implied a good repeatability of the measurements without applying a complicated pretreatment procedure to the electrode.

The reproducibility was also investigated with five different GCEs independently constructed by the same steps, as presented in Fig. S-4.† The RSD was 4.4% for the ΔR_{ct} to 1×10^{-8} M Ag^+, indicating that the fabrication procedure was reliable and that the modified GCE had good reproducibility. The long-term stability of the biosensor was investigated by the response to 1×10^{-8} M Ag^+ in 0.1 M PBS (pH 7.4) containing 5 mM $[Fe(CN)_6]^{3-/4-}$ (1 : 1) and 10 mM KCl for 1 month. When not in use, the electrode was stored in a moist state at 4 °C, and the current response was periodically measured. Beyond this period, the experiment was carried out per 10 days. The result showed that the biosensor retained about 85% of its original ΔR_{ct} after 1 month. The relatively good stability of the biosensor may be explained by the fact that the film (MCN and GNPs) could provide a biocompatible microenvironment, and the hairpin-like structure and the specific recognition ability to form C–Ag^+–C could be effectively protected.

The selectivity of this detection method is tested by substituting the Ag^+ in the system with various metal ions, which are commonly present in real samples such as Pb^{2+}, Cr^{3+}, Co^{2+}, Hg^{2+}, Cu^{2+}, Cd^{2+} and K^+. As shown in Fig. 6, each competing metal ion was tested at 1×10^{-6} M, 1×10^{-5} M, 1×10^{-4} M under the same experimental conditions. None of the corresponding ΔR_{ct} of the tested metal ions was higher than half of that produced by 1×10^{-8} M, 1×10^{-7} M, 1×10^{-6} M

Table 1 Comparison with other published Ag^+ detection sensor

Method	Materials	Linear range (mol L^{-1})	LOD (mol L^{-1})	References
The red-shift of the emission band of quantum dots (QDs)	CdTe	1.5×10^{-5}–1×10^{-7}	5×10^{-8}	31
Impedimetric immobilized DNA-based sensor for the detection of Ag^+	Gold electrode	1×10^{-7}–8×10^{-7}	1×10^{-8}	29
Colorimetric and ratiometric fluorescent chemosensor for the selective detection of Ag^+	Heptamethine cyanine	6×10^{-8}–5×10^{-6}	6×10^{-8}	32
Electrochemical sensing platform for Ag^+ detection	Multi-walled carbon nanotubes	1×10^{-8}–5×10^{-7}	1.3×10^{-9}	33
Colorimetric detection of Ag^+	Gold nanoparticles	—	3.3×10^{-9}	34
Oligonucleotide-based fluorogenic probe	Sybr Green I	5×10^{-8}–7×10^{-7}	3.2×10^{-8}	35
Magnified fluorescence detection of Ag^+	Nano-graphite–DNA hybrid and DNase I	—	3×10^{-10}	12
Colorimetric detection of Ag^+	Hemin DNAzyme	—	6.3×10^{-9}	36
Ion-selective electrodes detection of Ag^+	Ionophore-doped fluorous membranes	—	3.8×10^{-11}	38
A nanoparticle autocatalytic sensor for Ag^+ detection	*O*-Phenylenediamine	6×10^{-8}–6×10^{-5}	6×10^{-8}	37
Impedimetric biosensor based on duplex-like DNA scaffolds	Ordered mesoporous carbon nitride	10^{-10}–10^{-5}	5×10^{-11}	This work

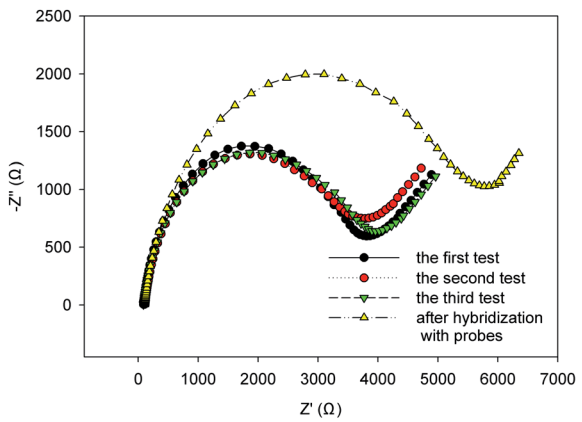

Fig. 5 The repeatability of the same biosensor for 1.0×10^{-8} M Ag^+ (different line represents different testing sample with the same biosensor).

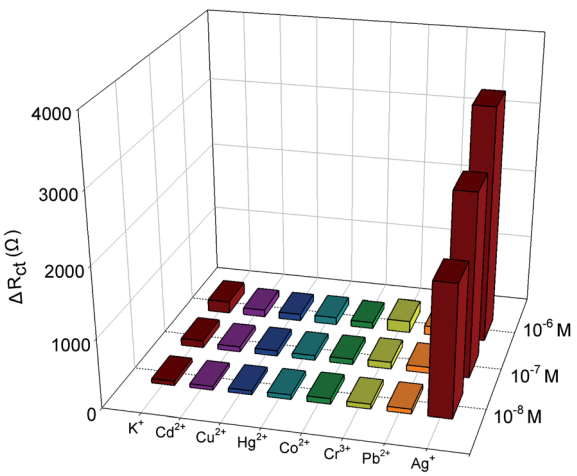

Fig. 6 Selectivity and interference study in the analysis of Ag^+ by the duplex-like DNA system. The data were averages of three replicate measurements.

Ag^+. Such an excellent selectivity is attributed to the specific C–Ag^+–C base pairing, which closely relates with signal change as mentioned above. The proposed biosensor exhibited good anti-interference ability and provided the potential to selectively determine Ag^+ levels in real samples.

Real samples detection

Five sewage samples were collected from a discharge outlet of untreated domestic sewage on the bank of Xiangjiang River, Hunan Province, and then were filtered through a 0.2 mM membrane to remove oils and other organic impurities. Subsequently, the sewage samples were spiked with a standard solutions of Ag^+ over the concentration range from 0.5 to 5000 nM prior to measurement. As seen in Table S-2,† the recoveries ranging from 95.2% to 105.8% after standard additions are satisfactory, suggesting that the biosensor could be efficiently used for the detection of Ag^+ content in the real samples.

Conclusion

In this paper, an unlabeled immobilized DNA-based sensor was reported to detect Ag^+ through the difference in charge-transfer resistance (ΔR_{ct}) before and after DNA interactions with Ag^+, which were monitored by electrochemical impedance spectroscopy (EIS). ΔR_{ct} is sufficiently sensitive to detect Ag^+ as low as 5×10^{-11} M with the linear range from 10^{-10} M to 10^{-5} M.

Moreover, because of the signal amplification by the MCN and GNPs platform and excellent specificity resulting from the hairpin-like DNA-based probes and the C–Ag^{+}–C interaction, the sensor maintained high selectivity over other nonspecific metal ions. It has good potential for application in environmental monitoring. Furthermore, alternative sensing devices for other metal ions may also be developed using other natural or synthetic specific hairpin-like probes.

Acknowledgements

The study was financially supported by the Young Top-Notch Talent Support Program of China (2012), the National Natural Science Foundation of China (51222805), the Program for New Century Excellent Talents in University from the Ministry of Education of China (NCET–11–0129), Interdisciplinary Research Project of Hunan University, China Scholarship Council (CSC) (2010843195), the Fundamental Research Funds for the Central Universities, Hunan University, and Hunan Provincial Innovation Foundation For Postgraduate (CX2009B080).

References

1 J. M. Liu, L. P. Lin, X. X. Wang, S. Q. Lin, W. L. Cai, L. H. Zhang and Z. Y. Zheng, *Analyst*, 2012, **137**, 2637–2642.
2 T. W. Purcell and J. J. Peters, *Environ. Toxicol. Chem.*, 1998, **17**, 539–546.
3 S. Kim, J. E. Choi, J. Choi, K. H. Chung, K. Park, J. Yi and D. Y. Ryu, *Toxicol. In Vitro*, 2009, **23**, 1076–1084.
4 J. L. Manzoori, H. Abdolmohammad-Zadeh and M. Amjadi, *J. Hazard. Mater.*, 2007, **144**, 458–463.
5 S. Ashoka, B. M. Peake, G. Bremner, K. J. Hageman and M. R. Reid, *Anal. Chim. Acta*, 2009, **653**, 191–199.
6 P. R. Aranda, P. H. Pacheco, R. A. Olsina, L. D. Martinez and R. A. Gil, *J. Anal. At. Spectrom.*, 2009, **24**, 1441–1445.
7 N. Pourreza, H. Parham, A. Kiasat, K. Ghanemi and N. Abdollahi, *Talanta*, 2009, **78**, 1293–1297.
8 I. Willner and M. Zayats, *Angew. Chem., Int. Ed.*, 2007, **46**, 6408–6418.
9 Y. Tanaka, S. Oda, H. Yamaguchi, Y. Kondo, C. Kojima and A. Ono, *J. Am. Chem. Soc.*, 2007, **129**, 244–245.
10 T. Li, S. Dong and E. Wang, *J. Am. Chem. Soc.*, 2010, **132**, 13156–13157.
11 A. Ono, S. Cao, H. Togashi, M. Tashiro, T. Fujimoto, T. Machinami, S. Oda, Y. Miyake, I. Okamoto and Y. Tanaka, *Chem. Commun.*, 2008, 4825–4827.
12 Y. Wei, B. Li, X. Wang and Y. Duan, *Biosens. Bioelectron.*, 2014, **58**, 276–281.
13 G. Xu, G. F. Wang, X. P. He, Y. H. Zhu, L. Chen and X. J. Zhang, *Analyst*, 2013, **138**, 6900–6906.
14 G. Liu, Y. Wan, V. Gau, J. Zhang, L. Wang, S. Song and C. Fan, *J. Am. Chem. Soc.*, 2008, **130**, 6820–6825.
15 S. Y. Niu, Q. Y. Li, R. Ren and S. S. Zhang, *Biosens. Bioelectron.*, 2009, **24**, 2943–2946.
16 P. Riccelli, F. Merante, K. Leung, S. Bortolin, R. Zastawny, R. Janeczko and A. S. Benight, *Nucleic Acids Res.*, 2001, **29**, 996–1004.
17 C. C. Chang, S. Lin, S. C. Wei, C. Y. Chen and C. W. Lin, *Biosens. Bioelectron.*, 2011, **30**, 235–240.
18 G. Xu, G. F. Wang, Y. H. Zhu, L. Chen, X. P. He, L. Wang and X. J. Zhang, *Biosens. Bioelectron.*, 2014, **59**, 269–275.
19 G. P. Yan, Y. H. Wang, X. X. He, K. M. Wang, J. Su, Z. F. Chen and Z. H. Qing, *Talanta*, 2012, **94**, 178–183.
20 S. H. Lee, C. K. Lee, S. R. Shin, B. K. Gu, S. Kim, T. M. Kang and S. J. Kim, *Sens. Actuators, B*, 2010, **145**, 89–92.
21 L. J. Yan, X. J. Bo, Y. F. Zhang and L. P. Guo, *Electrochim. Acta*, 2014, **137**, 693–699.
22 L. P. Lu, L. H. Xu, T. F. Kang and S. Y. Cheng, *Appl. Surf. Sci.*, 2013, **284**, 258–262.
23 Y. Y. Zhou, L. Tang, G. M. Zeng, J. Chen, Y. Cai, Y. Zhang, G. D. Yang, Y. Y. Liu, C. Zhang and W. W. Tang, *Biosens. Bioelectron.*, 2014, **61**, 519–525.
24 L. Tang, Y. Y. Zhou, G. M. Zeng, Z. Li, Y. Y. Liu, Y. Zhang, G. Q. Chen, G. D. Yang, X. X. Lei and M. S. Wu, *Analyst*, 2013, **138**, 3552–3560.
25 Y. Y. Zhou, L. Tang, G. M. Zeng, Y. Zhang, Z. Li, Y. Y. Liu, J. Chen, G. D. Yang, L. Zhou and S. Zhang, *Anal. Methods*, 2014, **7**, 2371–2378.
26 Y. Zhang, G. M. Zeng, L. Tang, Y. P. Li, L. J. Chen, Y. Pang, Z. Li, C. L. Feng and G. H. Huang, *Analyst*, 2011, **136**, 4204–4210.
27 T. H. M. Kjällman, H. Peng, C. Soeller and J. Travas-Sejdic, *Anal. Chem.*, 2008, **80**, 9460–9466.
28 L. Tang, G. M. Zeng, G. L. Shen, Y. P. Li, C. Liu, Z. Li, J. Luo, C. Z. Fan and C. P. Yang, *Biosens. Bioelectron.*, 2009, **24**, 1474–1479.
29 Z. Lin, X. Li and H. B. Kraatz, *Anal. Chem.*, 2011, **83**, 6896–6901.
30 Y. Wang, C. Li, X. Li, Y. Li and H. B. Kraatz, *Anal. Chem.*, 2008, **80**, 2255–2260.
31 J. Wang, J. Liang, Z. Sheng and H. Han, *Microchim. Acta*, 2009, **167**, 281–287.
32 H. Zheng, M. Yan, X. X. Fan, D. Sun, S. Y. Yang, L. J. Yang, J. D. Li and Y. B. Jiang, *Chem. Commun.*, 2012, **48**, 2243–2245.
33 G. Yan, Y. Wang, X. He, K. Wang, J. Su, Z. Chen and Z. Qing, *Talanta*, 2012, **94**, 178–183.
34 Y. M. Sung and S. P. Wu, *Sens. Actuators, B*, 2014, **197**, 172–176.
35 Y. H. Lin and W. L. Tseng, *Chem. Commun.*, 2009, **43**, 6619–6621.
36 X. H. Zhou, D. M. Kong and H. X. Shen, *Anal. Chim. Acta*, 2010, **678**, 124–127.
37 X. Yang and E. Wang, *Anal. Chem.*, 2011, **83**, 5005–5011.
38 C. Z. Lai, M. A. Fierke, R. C. da Costa, J. A. Gladysz, A. Stein and P. Bühlmann, *Anal. Chem.*, 2010, **82**, 7634–7640.